Available online at www.sciencedirect.com
SCIENCE DIRECT®
International Journal of Heat and Mass Transfer 48 (2005) 4300–4306
International Journal of HEAT and MASS TRANSFER
www.elsevier.com/locate/ijhmt

Constructal multi-scale cylinders with natural convection

T. Bello-Ochende [a,*], A. Bejan [b]

[a] Department of Mechanical and Aeronautical Engineering, University of Pretoria, 0002 Pretoria, South Africa
[b] Department of Mechanical Engineering and Materials Science, Duke University, P.O. Box 90300, Durham, NC 27708-0300, USA

Received 6 April 2005; received in revised form 27 May 2005
Available online 19 July 2005

Abstract

This paper shows that in a space filled with assemblies of cylinders cooled by natural convection the heat transfer density can be increased progressively by the use of cylinders of several sizes, and the optimal placement of each cylinder in the assembly. Smaller cylinders are placed closer to the entrance to the assembly, in the wedge-shaped flow regions occupied by fluid that has not yet been used for heat transfer. The paper reports the optimized flow architectures and performance for structures with one and two cylinder sizes, which correspond to structures with one and two degrees of freedom. The heat transfer rate density increases as the optimized structure becomes more complex. The optimized cylinder diameters are relatively robust, i.e., insensitive to changes in complexity and flow regime (Rayleigh number). The optimized spacings decrease monotonically as the Rayleigh number increases. The structure performance can be improved by endowing the cylinder assemblies with more degrees of freedom.

Keywords: Multi-scale design; Constructal; Horizontal cylinders; Natural convection

1. Introduction

The need to extract more and more heat from a given space has led to unconventional ways of designing structures for heat and fluid flow that maximize the rate of heat transfer from a given space. This has also been the driving force behind many of the miniaturization efforts and augmentation of heat transfer devices. The same trend is driven by the need to install more and more heat generating components into a given space. This activity has been described recently as a principle-based constructal process [1] of generating flow architecture in the pursuit of global objective, subject to global constraints. The flow configuration is the unknown.

The strategy is to endow the flow configuration with the freedom to change, and to search systematically for paths that lead to optimal or near-optimal flow configurations. Strategy and systematic search mean that architectural features that have been found beneficial in the past can be incorporated and compounded into more complex flow structures of the present. Strategy is important not only for accelerating the search in a design space that is infinite, but also for identifying the near-optimal designs that perform at nearly the same level as the absolute best. The increasing availability of inexpensive and reliable numerical packages means that complex optimization of convective flows (free and forced convection) which are often more difficult to program has now become more common.

* Corresponding author. Tel.: +27 12 420 3105; fax: +27 12 362 5124.
E-mail address: tbochende@tuks.co.za (T. Bello-Ochende).

0017-9310/$ - see front matter © 2005 Elsevier Ltd. All rights reserved.
doi:10.1016/j.ijheatmasstransfer.2005.05.023

Nomenclature

D_0	diameter
k	thermal conductivity (W/mK)
H_d	downstream flow length (m)
H_u	upstream flow length (m)
P	pressure (Pa)
Pr	Prandtl number
q	total heat transfer (W)
$\tilde{q}$	dimensionless heat transfer density, Eq. (12)
q''	heat transfer rate per unit length (W/m)
q'''	heat transfer rate density (W/m^3)
Ra	Rayleigh number, Eq. (7)
S_0	spacing between D_0 cylinders
T	temperature (K)
T_w	wall temperature (K)
T_0	inlet temperature (K)
u, v	velocity components (m/s)
x, y	Cartesian coordinates (m)

Greek symbols

α	thermal diffusivity (m^2/s)
μ	viscosity (kg/sm)
v	kinematic viscosity (m^2/s)
ρ	density (kg/m^3)

Subscripts

m	maximized once
2m	maximized twice
opt	optimum
w	wall

Superscript

(∼)	dimensionless variables, Eqs. (5) and (6)

One class of heat and fluid flow structures that have been optimized in this spirit are the configurations in which optimal spacings exist: stacks of parallel plates, staggered plates, cylinders in cross-flow, and pin fin arrays with impinging flow. Optimal spacings have been determined for natural convection, and for forced convection with specified overall pressure difference. This work has been reviewed in Refs. [1–3], and is not reviewed again here. It has one important characteristic that links all the optimized configurations: the optimized spacing is a *single* length scale that is distributed *uniformly* throughout the given volume.

In this paper, we propose to go beyond the single-spacing philosophy, and to explore the idea of optimizing flow structures with more than one free length scale. This direction of thought has a lot in common with the most recent work on tree-shaped flow structures [1–14] where the length scales are numerous, hierarchically organized and nonuniformly distributed through the available space. In the present paper, the multiple length scales are the diameters and spacings between cylinders cooled by natural convection. The largest cylinder diameter defines the overall extent of the flow space. The nonuniform distribution of these length scales means that progressively smaller cylinders are placed near the entrance to the assembly, i.e., in flow regions inhabited by fluid that has not participated in the global heat transfer enterprise.

2. Model

Consider the row of parallel cylinders shown in Fig. 1. The length of the assembly L and the cylinder diameter D_0 are fixed. The first objective is to select the number of cylinders in the bundle, or the cylinder-to-cylinder spacing, S_0, such that the overall thermal conductance between the cylinder and the ambient air is maximal. The flow is assumed steady, laminar, incompressible and two dimensional. All the thermophysical properties are assumed constant. The temperature variations are sufficiently small relative to the absolute temperature so that Boussinesq approximation is valid.

The lower part of Fig. 1 shows the elemental volume that characterizes this assembly. Symmetry allows us to study only half of the channel formed between two cylinders. The computational domain contains the flow region of length D_0, plus an upstream section $H_u \times \frac{1}{2}(D_0 + S_0)$, and a downstream section $H_d \times \frac{1}{2}(D_0 + S_0)$. The lengths H_u and H_d were selected based on accuracy tests described later in this section.

The conservation equations for mass, momentum and energy are

$$\frac{\partial u}{\partial x} + \frac{\partial v}{\partial y} = 0 \tag{1}$$

$$u\frac{\partial u}{\partial x} + v\frac{\partial u}{\partial y} = -\frac{1}{\rho}\frac{\partial P}{\partial x} + v\nabla^2 u \tag{2}$$

$$u\frac{\partial v}{\partial x} + v\frac{\partial v}{\partial y} = -\frac{1}{\rho}\frac{\partial P}{\partial y} + v\nabla^2 v + g\beta(T - T_\infty) \tag{3}$$

$$u\frac{\partial T}{\partial x} + v\frac{\partial T}{\partial y} = \alpha\nabla^2 T \tag{4}$$

where $\nabla^2 = \partial^2/\partial x^2 + \partial^2/\partial y^2$. The system of coordinates (x, y) and the velocity components (u, v) are defined in

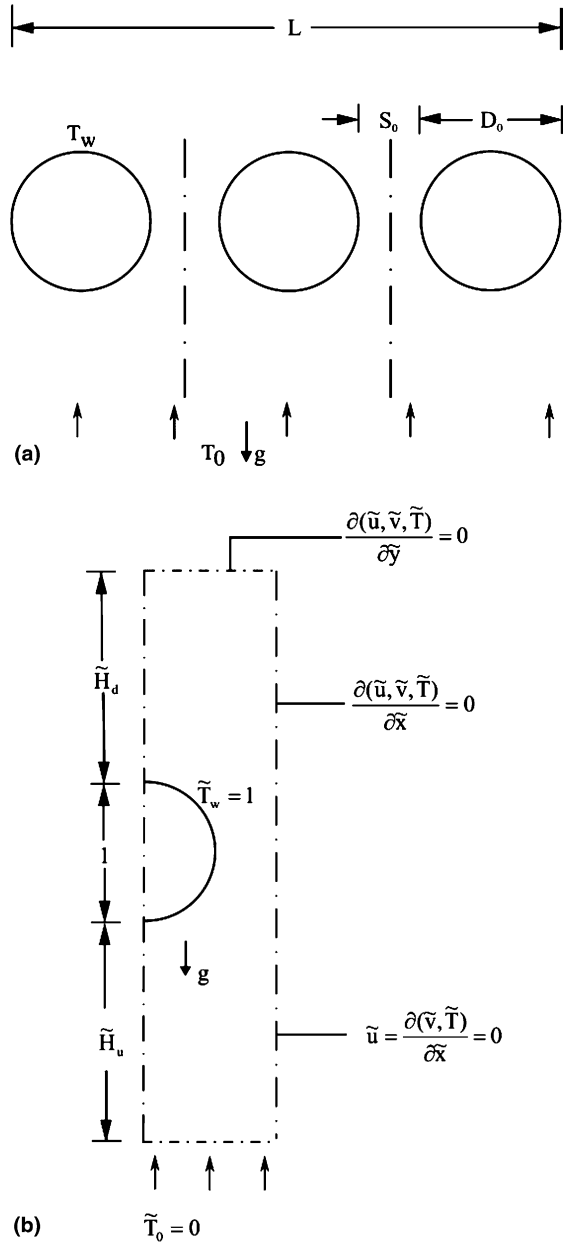

Fig. 1. Single row of cylinders in natural convections, and the computational domain.

Fig. 1. The variables are defined in Nomenclature. The numerical work of solving Eqs. (1)–(4) is based on a dimensionless formulation using the variables

$$(\tilde{x},\tilde{y})=\frac{(x,y)}{D_0},\quad (\tilde{u},\tilde{v})=\frac{(u,v)}{\alpha\mu/(Ra_{D_0}Pr)^{1/2}} \tag{5}$$

$$\tilde{T}=\frac{T-T_\infty}{T_w-T_\infty},\quad \tilde{P}=\frac{PD_0^2}{\mu\alpha/(Ra_{D_0}Pr)^{1/2}} \tag{6}$$

where Ra is the Rayleigh number,

$$Ra=\frac{g\beta L^3(T_w-T_\infty)}{\alpha\nu} \tag{7}$$

The Prandtl number is $Pr=\nu/\alpha$. The dimensionless version of Eqs. (1)–(4) is

$$\frac{\partial\tilde{u}}{\partial\tilde{x}}+\frac{\partial\tilde{v}}{\partial\tilde{y}}=0 \tag{8}$$

$$\left(\frac{Ra}{Pr}\right)^{1/2}\left(\tilde{u}\frac{\partial\tilde{u}}{\partial\tilde{x}}+\tilde{v}\frac{\partial\tilde{u}}{\partial\tilde{y}}\right)=-\frac{\partial\tilde{P}}{\partial\tilde{x}}+\nabla^2\tilde{u} \tag{9}$$

$$\left(\frac{Ra}{Pr}\right)^{1/2}\left(\tilde{u}\frac{\partial\tilde{v}}{\partial\tilde{x}}+\tilde{v}\frac{\partial\tilde{v}}{\partial\tilde{y}}\right)=-\frac{\partial\tilde{P}}{\partial\tilde{x}}+\nabla^2\tilde{v}+\left(\frac{Ra}{Pr}\right)^{1/2}\tilde{T} \tag{10}$$

$$(RaPr)^{1/2}\left(\tilde{u}\frac{\partial\tilde{T}}{\partial\tilde{x}}+\tilde{v}\frac{\partial\tilde{T}}{\partial\tilde{y}}\right)=\nabla^2\tilde{T} \tag{11}$$

The flow boundary conditions are indicated in Fig. 1b: no slip and no penetration on the plate surfaces; $\tilde{P}=0$, $\tilde{u}=\partial\tilde{v}/\partial\tilde{y}=0$ at the inlet of the computational plane; $\tilde{P}=0$ and $\partial(\tilde{u},\tilde{v})/\partial\tilde{y}=0$ at the exit of the computational domain; and free slip and no penetration ($\tilde{u}=\partial\tilde{v}/\partial\tilde{y}=0$) at the upstream section of the computational domain ($0\leqslant\tilde{y}\leqslant H_u$). For the downstream section ($H_u+\tilde{D}_0\leqslant\tilde{y}\leqslant H_u+\tilde{D}_0+H_d$) we specified two flow boundary conditions: free slip and no penetration ($\tilde{u}=\partial\tilde{v}/\partial\tilde{x}=0$) on the left side of the downstream section of the computational domain, and zero stress [$\partial(\tilde{u},\tilde{v})/\partial\tilde{x}=0$] on the right side of the downstream section of the domain. By specifying $\partial\tilde{u}/\partial\tilde{x}=0$ on this side we allow fluid to flow horizontally into the computational domain. This entrainment effect nullifies the unrealistic vertical acceleration (chimney effect) that would have been generated had we imposed no-slip on that side. The thermal boundary conditions are $\tilde{T}=1$ on the plate surfaces, and $\tilde{T}=0$ on the inlet plane of the computational domain. The remaining portions of the computational domain were modeled as adiabatic.

The spacing between cylinders varies. We are interested in the geometric arrangement that maximizes the overall heat transfer between the cylinder and the surrounding fluids. The dimensionless quantity that is used to determine this arrangement is the dimensionless heat transfer rate density. The heat transfer density rate is $q'''=q'/[D_0(D_0+S_0)]$, where q' is the total heat transfer rate integrated over the surface of one cylinder. The corresponding q''' in the dimensionless form is

$$\tilde{q}=\frac{q'}{D_0(D_0+S_0)k(T_w-T_0)} \tag{12}$$

3. Numerical method

Eqs. (8)–(10) were solved using a finite element code with four-node quadrilateral elements and linear interpolation functions [16]. The explicit appearance of the

Table 1
Grid refinement tests for calculation of $\tilde{q}$ when $\tilde{S}_0 = 0.3$, $Ra = 10^3$, $Pr = 0.72$

Number of nodes per D_0 in the $\tilde{x}$ and $\tilde{y}$ directions	$\tilde{q}$	$\left\lvert\frac{\tilde{q}^i - \tilde{q}^{i+1}}{\tilde{q}^i}\right\rvert$
10	5.9035	–
20	5.9163	0.0021
40	5.9266	0.0017
80	5.9319	0.00087

pressure in the momentum equation was eliminated by using the penalty function method. In all the simulations the compressibility parameter was fixed at 10^{-8}. For more details see Ref. [17]. The nonlinear equations resulting from the Galerkin finite-element discretization of Eqs. (8)–(10) were solved using successive substitution followed by a quasi-Newton method. The convergence criteria were

$$\frac{\|u^{(k)} - u^{(k-1)}\|}{\|u^k\|} \leqslant 10^{-3} \text{ and } \frac{\|R(u^{(k)})\|}{\|R_0\|} \leqslant 10^{-3} \tag{13}$$

in which $R(u)$ is the residual vector, u is the complete solution vector, k is the iteration counter, and $\|\cdot\|$ is the Euclidian norm. The grid was non-uniform in both $\tilde{x}$ and $\tilde{y}$ directions. The grid was double graded in the $\tilde{x}$ direction so as to put more nodes near the cylinder surfaces to capture more accurately the behavior in the boundary layers. The grid varied from one geometric configuration to another. Grid refinement tests performed in range ($10^3 \leqslant Ra \leqslant 10^5$, $Pr = 0.72$) indicated that the solutions were insensitive to further grid doubling in $\tilde{x}$ and $\tilde{y}$ when 40 nodes per D_0 were used in both $\tilde{x}$ and $\tilde{y}$ directions. Table 1 shows how grid independence was achieved. Another set of accuracy tests showed that when $H_u/D_0 = 1.0$ and $H_d/D_0 = 1.5$, the channel heat transfer rate varied less than 1% after the doubling of the upstream and downstream lengths. Based on these tests, the numerical results discussed in this paper we obtained with grids of 40 nodes per D_0, and with $\tilde{H}_u = 1.0$ and $\tilde{H}_d = 1.5$.

4. Numerical results and scale analysis

The flow and temperature fields were simulated in a large number of configurations, in order to determine the effect of spacing on heat transfer density. Fig. 2 shows that the heat transfer density is maximal when S_0 has a certain value. The optimal spacings determined in this manner are summarized in Fig. 3, which shows that for $Pr = 0.72$ they are correlated within 0.002% by the power law

$$\frac{S_{opt}}{D_0} = 1.32Ra^{-0.22} \tag{14}$$

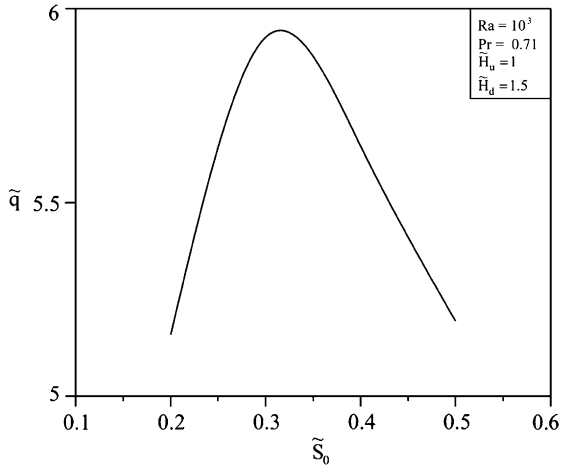

Fig. 2. The maximization of heat transfer density in the assembly of Fig. 1.

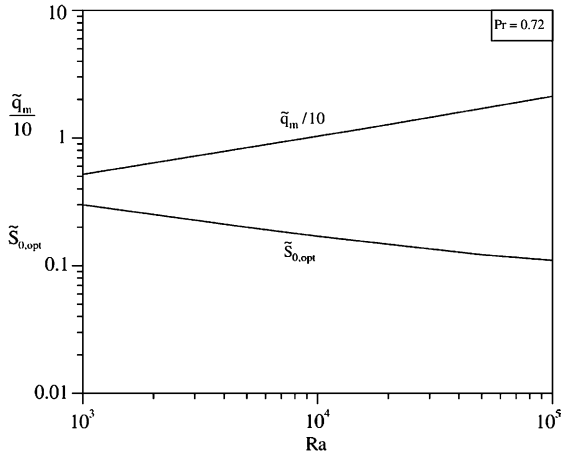

Fig. 3. The optimal spacing and maximal heat transfer density for the row of cylinders shown in Fig. 1.

The corresponding heat transfer density maxima are reported in Fig. 3. They are correlated within 0.003% by the expression

$$\tilde{q}_m = 0.65Ra^{0.30} \tag{15}$$

These results are in agreement with the constructal method (Ref. [1], Chapter 3), according to which maximal heat transfer density means 'optimal packing' such that flow regions that do not contribute to global performance are eliminated. This means that optimal packing in Fig. 1 is achieved when the cylinders are brought close enough so that their thermal boundary layers just touch. According to scale analysis the thermal boundary layer of a cylinder with laminar natural convection flow and $Pr > 1$ [15] has a thickness of order

$$\delta_T \sim D_0 Ra^{-1/4} \tag{16}$$

By setting $\delta_T \sim S_0$ in Eq. (16), we find that

$$\tilde{S}_0 \sim Ra^{-1/4} \tag{17}$$

which anticipates very well the numerical correlation (14).

The heat transfer rate density (15) can be anticipated based on the same scaling argument. The cylinder heat flux scale is $q'' \sim k(T_w - T_0)/\delta_T$, where $\delta_T \sim S_0 \sim D_0\tilde{S}_0$. Because $S_0 < D_0$, cf. Eq. (16) for $Ra \gg 1$, the heat transfer rate density is $q''' \sim q''/D_0$, such that the dimensionless heat transfer rate density becomes,

$$\tilde{q} \sim \frac{q'''D_0^2}{k(T_w - T_0)} \sim Ra^{1/4} \tag{18}$$

This formula anticipates very well the numerical correlation, Eq. (15).

5. Increasing complexity

In the second phase of this study, we considered the more complex structure shown in Fig. 4. Cylinders of smaller diameter (D_1) were inserted in the entrance (converging) regions of the channels formed between the original cylinders. This structural change brings one more degree of freedom: the small-cylinder diameter $\tilde{D}_1 = D_0/D_1$. The flow configuration has two degrees of freedom, which are represented by $\tilde{D}_1$ and the original spacing $\tilde{S}_0$.

The numerical procedure for flow simulation and geometry optimization was the same as the procedure tested in Section 2. As shown in the example of Fig. 5,

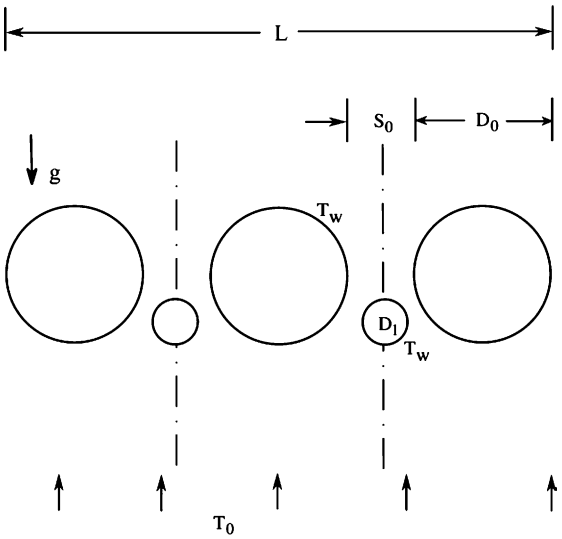

Fig. 4. Row of cylinders with two sizes (two degrees of freedom).

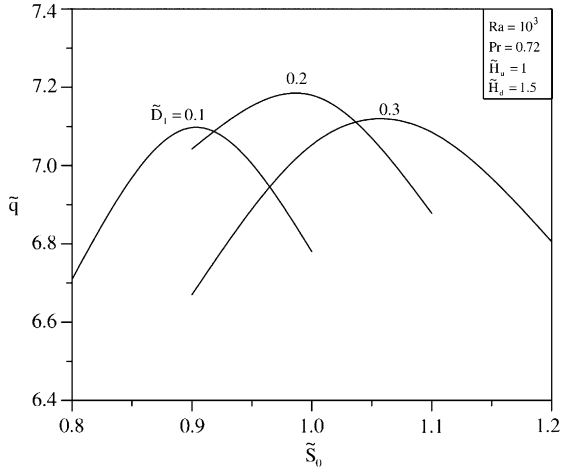

Fig. 5. The maximization of heat transfer density in the assembly of Fig. 4.

the Ra number was fixed, and many configurations $(\tilde{D}_1, \tilde{S}_0$ were simulated in the search for the configuration with the highest heat transfer density $\tilde{q}$. This procedure was then repeated over the range $10^3 \leqslant Ra \leqslant 10^5$ and $Pr = 0.72$.

The results are condensed in Fig. 6, which shows how the optimized configuration and the maximized performance vary with the Rayleigh number. The optimal small diameter is independent of Ra: the optimal ratio D_1/D_0 is practically constant and equal to 0.20. The optimal spacing decreases as Ra increases. This behavior is consistent with what we saw in Fig. 3, however the $\tilde{S}_{0,opt}$ values of Fig. 6 are consistently larger than the optimal spacings reported in Fig. 3. The optimal spacing is larger when a smaller cylinder is placed in the mouth of the channel. The data of Figs. 3 and 6 show that the

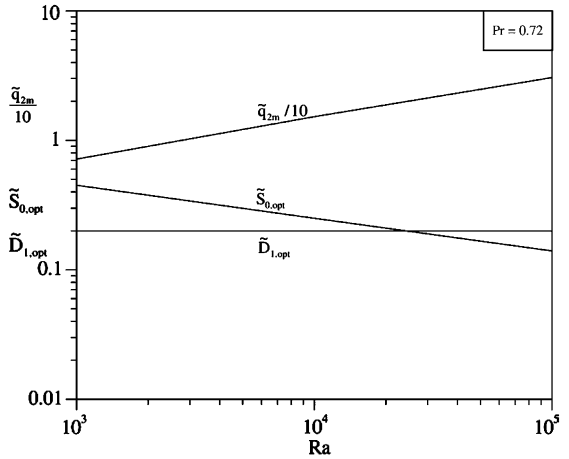

Fig. 6. The optimal spacing, optimal diameter ratio $\tilde{D}_1$ and maximal heat transfer density for the assembly shown in Fig. 4.

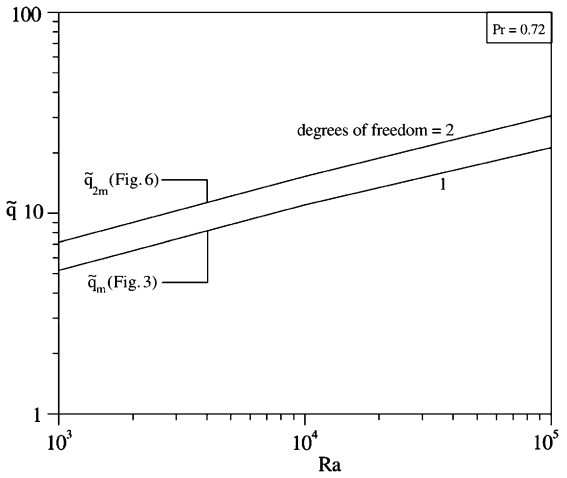

Fig. 7. The effect of the increasing complexity on the maximum heat transfer rate density.

ratio of the optimized spacings is practically independent of Ra,

$$\frac{\tilde{S}_{0,\mathrm{opt}}(\mathrm{Fig.6})}{\tilde{S}_{0,\mathrm{opt}}(\mathrm{Fig.3})} \cong 1.68 \tag{19}$$

The maximized heat transfer density shown in Fig. 6 increases with Ra. This trend is qualitatively in agreement with the results obtained for single-scale structures (Fig. 3). The subscript 2m is a reminder that $\tilde{q}$ was maximized with respect to two geometric parameters, $\tilde{S}_0$ and $\tilde{D}_1$. In place of Eq. (15), the $\tilde{q}_{2m}$ data of Fig. 6 are correlated within 0.06% by the power law $\tilde{q}_{2m} = 0.85Ra^{0.3}$. It can be verified that $\tilde{q}_{2m}(\mathrm{Fig.6}) > \tilde{q}_{m}(\mathrm{Fig.3})$, which means that the use of two scales (D_0, D_1) brings about an increase in heat transfer rate density. This finding is summarized in Fig. 7, which shows that the maximized heat transfer rate density increases as the number of geometric degrees of freedom increases or as one additional cylinder is inserted between the flow structure surrounding the larger cylinder.

6. Conclusions

In this paper we illustrated a new approach to the conceptual design of convective structures with maximal heat transfer density: the use of multiple length scales that are distributed nonuniformly through the available volume. For illustration, we used parallel cylinders in natural convection. We installed new cylinders with progressively smaller diameters in the entrance wedges between older cylinders, where the flow regions were inhabited by fluid that had not been used for heat transfer.

Two classes of configurations were optimized and reported: cylinders with one and two sizes, which resided in flow structures with one and two degrees of freedom. The maximized heat transfer density increases from one class to the next. The optimized cylinder diameters are robust, i.e., relatively insensitive to changes in the number of scales and the flow regime (Ra).

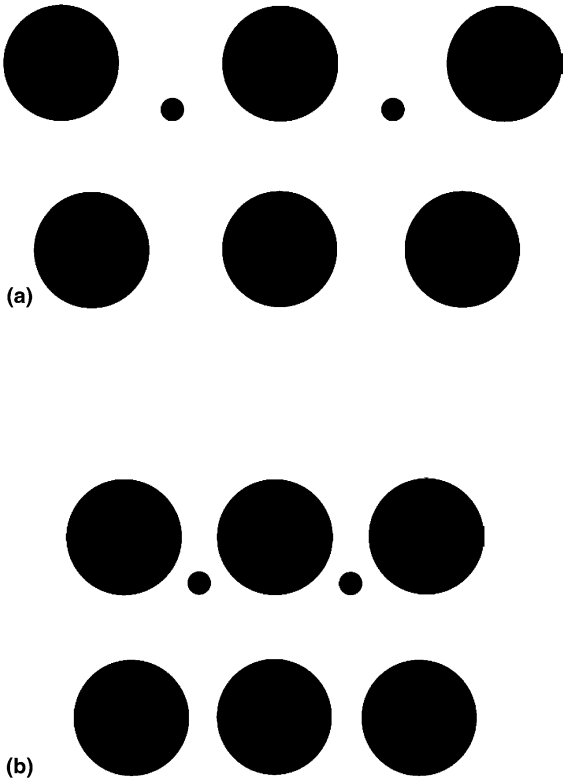

Fig. 8. The effect of increasing complexity and Rayleigh number (Ra) on the optimized multi-scale structure: (a) $Ra = 10^3$; and (b) $Ra = 10^5$.

In Fig. 8a and b, we drew to scale the optimized flow architectures with one and two freely varying length scales, cf. Figs. 1 and 4 respectively. Fig. 8 shows how the spacing between older cylinders increases when new cylinders are placed in the existing gaps. Read from Fig. 8a and b, the montage shows that when the flow becomes faster the spacings become noticeably smaller, while the cylinder diameters do not change much.

This last observation is relevant not only in heat exchanger design but also in animal design. A morphing multi-scale structure is robust when it can perform optimally under different flow conditions (slow, fast) by using the same solid parts. It is a lot easier for the structure to adapt itself by optimizing its fluid spacings, as opposed to redesigning its solid components. One example from the animal realm is the multi-channel organization of a swarm of bees [18]. The solid components (the bees) are permanent features, while the airways change

with the inlet temperature of the ambient air that cools the swarm (see also Ref. [1], pp. 44–45).

Acknowledgement

The authors want to thank Prof. J. P. Meyer and Prof. Leon Liebenberg (University of Pretoria, South Africa) for their constant support.

References

[1] A. Bejan, Shape and Structure from Engineering to Nature, Cambridge University Press, Cambridge, UK, 2000.
[2] A. Bejan, S. Lorente, The constructal law and the thermodynamics of flow systems with configuration, Int. J. Heat Mass Transfer 47 (2004) 3203–3214.
[3] A. Bejan, S. Lorente, La Loi Constructale, L' Harmattan, Paris, 2005.
[4] D.V. Pence, Reduced pumping power and wall temperature in microchannel heat sinks with fractal-like branching channel networks, Microscale Thermophys. Eng. 6 (2002) 319–330.
[5] Y. Chen, P. Cheng, Heat transfer and pressure drop in fractal tree-like microchannel nets, Int. J. Heat Mass Transfer 45 (2002) 2643–2648.
[6] Z.-Z. Xia, Z.-X. Li and Z.-Y. Guo, Heat conduction optimization: high conductivity constructs based on the principle of biological evolution, 12th International Heat Transfer Conference, Grenoble, France, 18–23 Aug, 2002.
[7] T. Bello-Ochende, A. Bejan, Maximal heat transfer density: Plates with multiple lengths in forced convection, Int. J. Therm. Sci. 43 (2004) 1181–1186.
[8] A.K. da Silva, A. Bejan, Constructal multi-scale structure for maximal heat transfer density in natural convection, Int. J. Heat Fluid Flow 26 (2005) 34–44.
[9] T. Bello-Ochende, A. Bejan, Constructal multi-scale cylinders in cross-flow, Int. J. Heat Mass Transfer 48 (2005) 1373–1383.
[10] D. Tondeur, L. Luo, U. D'Ortona, Optimisation des transferts et des materiaux par l'approche constructale, Entropie 30 (2000) 32–37.
[11] M.-O. Coppens, Y. Cheng and C.M. van den Bleek, Controlling fluidized bed operation using a novel hierarchical gas injection system, Paper 304d, AIChE Annual Meeting, Dallas, TX, 31 Oct–5 Nov, 1999.
[12] H. Brod, Residence time optimised choice of tube diameters and slit heights in distribution systems for non-Newtonian liquids, J. Non-Newtonian Fluid Mech. 111 (2003) 107–125.
[13] T. Borrvall, A. Klarbring, J. Petersson, B. Torstenfelt, Topology optimization in fluid mechanics, in H.A. Mang, F.G. Rammerstorfer, J. Eberhardsteiner (Eds.), Proceedings of the 5th WCCM V, World Congress on Computational Mechanics, Vienna, 7–12 July, 2002.
[14] T. Furukawa, W.-J. Yang, Thermal optimization of channel flows with discrete heating sections, J. Non-Equil. Thermody. 28 (2003) 299–310.
[15] A. Bejan, Convection Heat Transfer, third ed., Wiley, New York, 2004.
[16] FIDAP Theory Manual, Fluid Dynamics International, Evanston, IL, Revision 8.6 (1998).
[17] J.N. Reddy, D.K. Gartling, The Finite Element Method in Heat Transfer and Fluid Dynamics, CRC Press, Boca Raton, FL, 1994.
[18] B. Heinrich, The mechanisms and energetics of honeybee swarm temperature regulation, J. Exp. Biol. 91 (1981) 25–55.